IFSA

Sergey Y. Yurish
Editor

Advances in OPTICS

Reviews

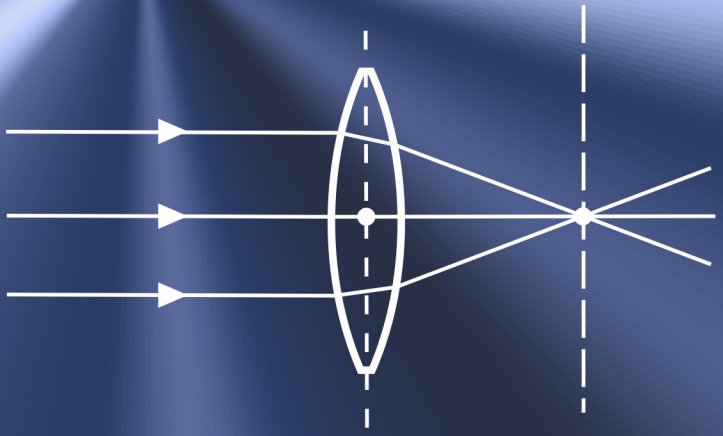

1

Sergey Y. Yurish
Editor

Advances in Optics: Reviews
Book Series, Vol. 1

Published by International Frequency Sensor Association (IFSA) Publishing, S. L., 2018
E-mail (for print book orders and customer service enquires): ifsa.books@sensorsportal.com

Visit our Home Page on http://www.sensorsportal.com

ISBN: 978-84-697-9435-7,
e-ISBN: 978-84-697-9436-4
BN-20180415-XX
BIC: TTB

Chapter 7
Vectorial Complex Ray Model for Light Scattering of Nonspherical Particles

Kuan Fang Ren and Claude Rozé

7.1. Introduction

Geometrical optics is a very simple and intuitive method for treating the interaction of an object with light or electromagnetic waves when the dimension of the object is much larger than the wavelength [1, 2]. One of its main advantages over the other methods is that it can be applied to objects of complex shape, which are hard or even impossible to be dealt with by rigorous theories or most numerical techniques. The variable separation methods based on the solution of Maxwell equations (or its equivalents) are limited to objects that can be described in a coordinate system of the same geometry, such as sphere, spheroid, ellipsoid, or circular or elliptical cylinder. Even in these "simple" cases, the numerical calculation remains another obstacle. Except for the sphere and the infinite circular cylinder, the calculable size of the scatterer can hardly exceed a few tens of wavelengths. Numerical methods such as T matrix, discrete multipole approximation, etc., can be applied to non - spherical particles, but the size parameter of the scatter is also severely limited [3].

Many researchers have contributed to the improvement of geometrical optics. Some take into account the forward diffraction or other particular wave effects (Airy theory for the rainbow [4] and Marston's model for the critical scattering [5]). Others combine directly geometrical optics with the electromagnetic wave method [6]. However, in these studies interference effects of all order rays are rarely taken into account. We have shown that, by taking into account the interferences between all scattered rays, as well as forward diffraction, we can predict correctly the scattering diagram of a sphere in all directions [7, 8], although the scattering diagram near the critical and rainbow angles is still to be improved. But, as soon as the geometrical optics is extended to a three - dimensional (3D) object of irregular shape, three difficulties are encountered: (1) calculation of local

Kuan Fang Ren
Rouen University, CORIA / UMR 6614, CNRS – INSA & Université de Rouen Normandie,
Saint Etienne du Rouvray, France

divergence factors for smooth dielectric surfaces; (2) phase shift due to focal lines; and (3) determination of reflection and refraction angles. If the last one concerns just a technical realization, the two others are inherent problem of ray models. To overcome these obstacles, we have been developing a so - called Vectorial Complex Ray Model (VCRM) in which the wave front curvature is introduced as an intrinsic property of a ray [9]. The calculation of the divergence factor in VCRM is just the ratio of the Gauss curvatures of the wave front surfaces and the phase shift due to the focal line is a count of the sign changes of the wave front curvature radii [10]. The direction of a ray and the Fresnel coefficients are determined simply by the tangent and normal components of the wave vector. The total scattered field is the superposition of the contributions of all complex rays. This model makes it possible to calculate the scattering of any irregularly shaped 3D objects illuminated by a plane wave or a shaped beam. In this chapter, we present the fundamentals of VCRM for an irregularly shaped 3D object, its applications to the scattering of non - spherical particles and characterization of liquid droplets in fluid mechanics.

The structure of the chapter is as follows. In Section 7.2, the fundamentals of geometrical optics and its applications to the scattering of a sphere or an infinite circular cylinder are presented in a way to ease the understanding of VCRM. Section 7.3 is devoted to the description of the Vectorial Complex Ray model, including its fundamental laws and its applications in simple cases of image formation to illustrate its power. The application of VCRM in the light scattering by an elliptical cylinder and a spheroidal particle in a symmetric plane is given in Section 7.4. The last section is the conclusions.

7.2. Fundamentals of Geometrical Optics

In this section we will present the essence of the geometrical optics (GO), or ray model in general sense, then apply it in the light scattering by particles and show that this model can predict very precisely the scattering diagram of a sphere or an infinite cylinder of circular section. These simple cases are very helpful to understand the Vectorial Complex Ray Model.

In ray models, a wave is considered as bundles of rays and each ray is characterized by four parameters.

The direction is usually described by an angle relative to the normal of the diopter. This is sufficient since the incident, reflected and refracted rays remain all in the same plane, called incident plane which is defined by the incident ray and the normal of the diopter.

The amplitude of the wave represented by the ray changes each time it is reflected or refracted by a diopter. It decreases when the light propagates in an absorbing medium. The amplitude evolves also along its path when the wave is convergent or divergent.

The polarization state of the light representing the vibration direction of the electric field is essential in the determination of the amplitudes of reflected and refracted waves by Bresnel coefficients.

The phase of the ray plays an important role in the interference of different orders if the coherent length of the incident wave is larger than the dimension of the particle. The interference can be constructive or destructive according to the phases of the rays. The three main factors which contribute to the phase of a ray are the optical path, the focal line/point and the Fresnel reflection coefficients.

We will see that careful count of these parameters permits to describe well the interaction of light with particle. A detailed description of these parameters will be given later. A special attention is payed to the scattering of light by particle. The sphere and the infinite circular cylinder are taken as examples to show that GO can be applied to deal with the scattering of light with good precision if all the properties are correctly counted. Unfortunately, they are also the only cases that can be treated "rigorously" in the scope of classical ray model. The barrier relies on the fact that in the classical ray model there is no parameter to take into account the divergence/convergence of the wave the rays represent. This will be possible with VCRM described in the next section.

7.2.1. Snell Laws and Fresnel Formulas

In the regime of ray model, the wavelength is much greater than the dimension of the object, the diopter surface can be considered as a plane tangent to the surface (here the convergence of the wave is not concerned). The directions of the reflected and refracted rays are related to that of the incident ray and the relative refractive index between the two media according to the Snell law.

$$\theta_i = \theta_l\,, \tag{7.1}$$

$$\sin\theta_i = m\sin\theta_r\,, \tag{7.2}$$

where θ_i, θ_l and θ_r are the incident angle, the reflection angle and the refraction angle respectively (Fig. 7.1).

The amplitude of the reflected wave and the refracted wave relative to the incident amplitude are given by the Fresnel formulas according to the state of polarization:

$$r_\perp = \frac{E_\perp^l}{E_\perp^i} = \frac{\cos\theta_i - m\cos\theta_r}{\cos\theta_i + m\cos\theta_r} = -\frac{\sin(\theta_i - \theta_r)}{\sin(\theta_i + \theta_r)}\,, \tag{7.3}$$

$$t_\perp = \frac{E_\perp^r}{E_\perp^i} = \frac{2\cos\theta_i}{\cos\theta_i + m\cos\theta_r} = \frac{2\sin\theta_r\cos\theta_i}{\sin(\theta_i + \theta_r)}\,, \tag{7.4}$$

$$r_\parallel = \frac{E_\parallel^l}{E_\parallel^i} = \frac{m\cos\theta_i - \cos\theta_r}{m\cos\theta_i + \cos\theta_r} = -\frac{\tan(\theta_i - \theta_r)}{\tan(\theta_i + \theta_r)}\,, \tag{7.5}$$

$$t_\parallel = \frac{E_\parallel^r}{E_\parallel^i} = \frac{2\cos\theta_i}{m\cos\theta_i + \cos\theta_r} = \frac{2\sin\theta_r\cos\theta_i}{\sin(\theta_i + \theta_r)\cos(\theta_i - \theta_r)}\,. \tag{7.6}$$

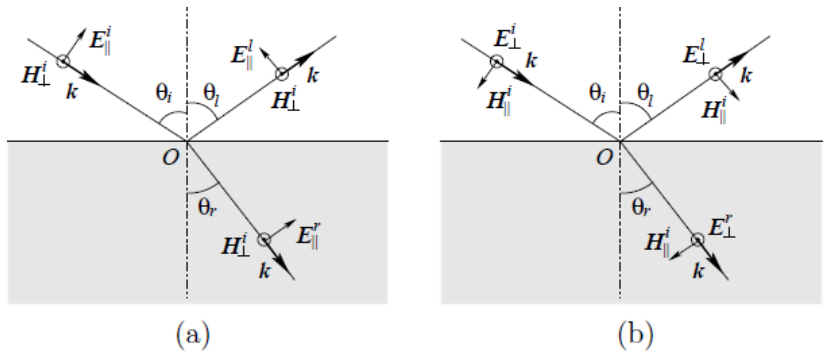

Fig. 7.1. Schema for derivation of Fresnel law.

The ratios of reflected and transmitted energy flux are described respectively by the reflectivity R_X and the transmissivity T_X:

$$R_X = |r_X|^2, \tag{7.7}$$

$$T_X = m\,|t_X|^2 \frac{\cos\theta_r}{\sin\theta_i}, \tag{7.8}$$

where the index X stands for the state of polarization: the electric field parallel || or perpendicular ⊥ to the incident plane. An attention should be paid to the fact that the transmissivity is not equal to the square of the amplitude ratio of the refracted (transmitted) wave to the incident wave.

7.2.2. Light Scattering by a Sphere and a Circular Cylinder

The geometrical optics is well known as a very simple and instructive method in dealing with the reflection and refraction of light from an object and widely used in the image formation. It has also been applied in some techniques for optical particle metrology, such as in the prediction of the positions of rainbow or the phase shift in the phase Doppler Anemometry. However, since longtime, the geometrical optics has been considered applicable only in narrow region in forward direction [11, 12]. In the early 2000's we have shown that the geometrical optics is capable to predict the scattering diagram of a sphere in all direction if the interference and diffraction effects are appropriately counted. This method can be easily extended to the scattering of a shaped beam [7, 8], or a multilayered sphere [12] or a cylinder [13]. However, it cannot be applied or extended to the particles without circular symmetry [14]. This will be the subject of the next section.

We deal with the scattering of plane wave by a homogeneous sphere and an infinite circular cylinder at normal incidence. These are the simplest scatterers, one in two dimensions and the other in three dimensions. Thanks to the symmetric property of the problem, the calculations of the deviation of the rays, the phases due to the optical path

and the amplitude ratios of reflection and refractions are the same at each interaction. These three aspects common to the two kinds of particle will be dealt with in the first subsection. The particular problems related to the shape of the particle, such as the phase due to the focal line, the divergence factor and the calculation of the total field will be discussed in the two subsections which follow.

7.2.2.1. Deviation of Rays on Particle Surface

Consider a particle having a circular section of radius a and refractive index m illuminated by a plane wave as shown in Fig. 7.2. The particle can be a sphere or an infinite circular cylinder of axis perpendicular to the plane of paper. We note the order of the emergent rays by p which indicates the emergent rays after $p + 1$ interactions with the particle surface. So the reflected ray corresponds to the order $p = 0$, the order of the first refracted rays is 1, and etc. Due to the symmetry of the problem, the angle of any emergent rays with the normal of the particle surface is constant and equal to the incident angle. The angle between any rays in the particle with the normal of the surface is also constant and equal to the refraction angle. Here we adopt the notations of van de Hulst [1] and note the angle between the incident ray and the tangent plane by τ and the angle between refracted ray and the tangent plane by τ'. They are related to the incident angle θ_i and the refraction angle θ_r by $\tau = \pi/2 - \theta_i$ and $\tau' = \pi/2 - \theta_r$.

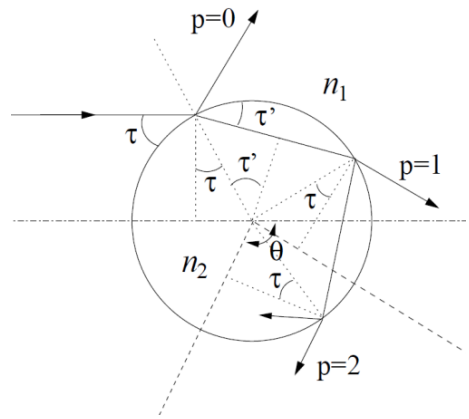

Fig. 7.2. Ray in a spherical/circular cylinder.

When a ray arrives at the surface of the particle, the reflected ray turns in the counterclockwise direction of an angle 2τ. The refracted ray of order p turns in clockwise direction an angle equal to p times $2\tau'$. The deviation angle is therefore given by

$$\theta = 2(\tau - p\tau') . \tag{7.9}$$

However, in practice, the scattered light is observed in 0 to 360°. More particularly, the scattering angle is usually scaled between 0 to 180° due to the symmetry of the sphere and the circular cylinder, and given by following relation

$$\theta_p = 2q_p(\tau - p\tau') + 2k_p\pi\,, \tag{7.10}$$

where k_p is the integer representing the times the emergent ray crosses the x axis and q_p takes + 1 or −1.

7.2.2.2. Amplitudes of Reflected and Refracted Rays

When a ray interacts with the surface of the particle, it is usually divided into two parts: reflected and refracted rays. The amplitudes of the reflected and refracted wave depend on the incident angle and the polarization of the incident wave. The ratios of the reflected and refracted wave amplitudes to the incident one are calculated by the Fresnel formula (7.3) - (7.6).

In the case under study, the Fresnel coefficients are constant for all orders of rays since the incident and refraction angles of all orders are the same. The reflection ratios on the outside of the particle surface are $r_\perp$ and $r_\parallel$ respectively for the two polarizations. The reflection ratios on the internal surface are the same as the first reflection, but the sign of both ratios are reversed, i.e. the two reflection ratios are respectively $-r_\perp$ and $-r_\parallel$. All orders of rays enter and exit one time the particle surface, so the refraction ratios are $1-r_\perp^2$ and $1-r_\parallel^2$. In summary, the ratio of the amplitude of the emergent wave of order p to the amplitude of the incident wave is given by

$$\varepsilon_{X,p} = \begin{cases} r_X & p = 0 \\ (1-r_X^2)(-r_X)^{p-1} & p \geq 1 \end{cases}, \tag{7.11}$$

where r_X stands for the reflection ratio of perpendicular polarization $r_\perp$ or of parallel polarization $r_\parallel$.

7.2.2.3. Phases of Rays

To take into account the interference between different orders or rays, the phase of the rays must be counted. The phase shifts of a ray can be classified into three kinds [1].

1. *Phase due to reflection and refraction* Φ_R: It is well known that when a wave is reflected on the surface from optically thinner medium to optically denser medium, there is a half - wave loss. In fact, this is true only when the incident angle is small. In more general case, this kind of phase shift is accounted in the Fresnel coefficients. When the total reflection occurs, the Fresnel coefficients are complex and the phase shift is to be deduced from the complex values of the coefficients.

2. *Phase due to optical path* Φ_P: This type of phase shift is due to the difference of optical path of rays and evaluated relatively to a reference. The usual reference taken in the literature and chosen here is the virtual ray which (i) propagates in surrounding medium (without any particle), (ii) arrives at the center in the same direction as the incident ray,

and (iii) exits in the same direction as the emergent ray. Therefore, the optical path of the reflected ray ($p = 0$) has a shorter path than the reference ray. This difference is equal to $2a\sin\tau$. Thus it has the positive phase shift equal to $2ka\sin\tau$. On the other hand, the rays of order $p \geq 1$ undergo $p-1$ reflections in the particle. The distance between two successive interactions of a ray with the particle surface is $2a\sin\tau'$, so the supplementary optical path relative to the reflection ray $p = 0$ is equal to $2apm\sin\tau'$. Therefore the phase shift due to the optical path is

$$\Phi_P = 2ka\left(\sin\tau - pm\sin\tau'\right). \tag{7.12}$$

3. *Phase due to focal lines* Φ_F: When a ray passes through a focal line, its phase advances by $\pi/2$[1]. The total phase shift due to focal lines depends on the order of the ray, the position of the ray and the shape of the particle. To illustrate the divergence and convergence of the bundle of rays, the trajectories of two adjacent rays impinging on a particle at different position are shown in Fig. 7.3. The focal lines of the rays (times the rays cross) in the plane of paper in Fig. 7.3(a) for $p = 0$ to 3 are respectively 0, 1, 1, 2 while the corresponding focal lines in Fig. 7.3(b) are 0, 1, 2, 3. In the cases of plane wave scattering by an infinite circular cylinder or a sphere, this phase shift can be calculated analytically according to the deviation of the rays. The details of the calculation will be given later in this section.

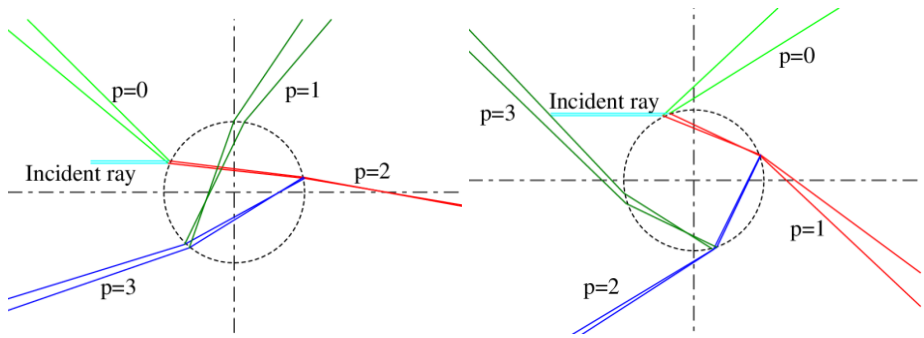

Fig. 7.3. Rays in a circular section.

The total phase of an emergent ray of order p is the summation of the three types:

$$\Phi_p = \Phi_R + \Phi_P + \Phi_F. \tag{7.13}$$

The two first phase shifts are the same for an infinite circular cylinder and a sphere while the last one depends on the shape of the particle. When the incident wave is not a plane wave, the phase of the incident wave must be counted also.

7.2.2.4. Scattering of an Infinite Circular Cylinder

When an infinite circular cylinder is illuminated by a plane wave, the scattering can be dealt with by tracing of rays in the circular section perpendicular to its symmetric axis. The waves being converged or diverged only in one direction, the phase shift due to the focal lines is given by [1]

$$\Phi_F = \frac{\pi}{2}\left[p - \frac{1}{2}(1-s) \right], \tag{7.14}$$

where s is the sign of the angle derivative $d\theta_p/d\tau$ that will be discussed later in this section.

When a wave arrives on a curved surface it will be converged or diverged. The amplitude of the reflected and the refracted wave will change consequently. This variation is described by the divergence factor according to the balance of the energy.

To determine the divergence factor, we consider an incident beam of section dA_i illuminating the particle surface of an area $dA = ad\tau dz$. All the flux in the beam spreads, after interactions with the particle, into an area dA_s in far distance r such that $dA_s = rd\theta dz$. Suppose that the intensity of the ray in far field is $I_p(\theta)$, then according to the energy balance we have $I_0 \varepsilon_{X,p}^2 a \sin\tau d\tau dz = I_p(\theta) r d\theta dz$. It follows that the scattered intensity of order p is given by

$$I_p(\theta) = \frac{\varepsilon_{X,p}^2 I_0 a \sin\tau d\tau}{r d\theta} = \frac{a}{r} I_0 \varepsilon_{X,p}^2 D, \tag{7.15}$$

where $\varepsilon_{X,p}^2$ is the coefficient related to the reflection on and transmission through the particle surface determined by the Fresnel formulas according to Eq. (7.11). The divergence factor D is defined by

$$D = \frac{\sin\tau}{|d\theta / d\tau|}. \tag{7.16}$$

The derivative $d\theta/d\tau$ is deduced from Eq. (7.9) and the Snell law (7.2), and is given by

$$\frac{d\theta}{d\tau} = 2\left(p\frac{\tan\tau}{\tan\tau'} - 1 \right). \tag{7.17}$$

The divergence factor is therefore

$$D = \frac{m\cos\theta_i \cos\theta_r}{2\left(p\cos\theta_i - m\cos\theta_r \right)}. \tag{7.18}$$

In the special case of external reflection ($p = 0$), the divergence factor is simplified to

$$D = \frac{\cos\theta_i}{2}. \tag{7.19}$$

It is independent of the refractive index as it should be.

7.2.2.5. Scattering of a Sphere

When a sphere is illuminated by a plane wave, the trajectories of rays are symmetric around the diameter along the incident direction and can be treated by ray tracing in the circular section. The calculation of the scattering angle and the phase due to the optical path are the same as for a circular cylinder discussed above. But the phase due to the focal points/lines and the divergence factor are different.

The focal lines in the scattering of a plane wave by a sphere can be classified into two sets according to van de Hulst [1]. The first set, noted by set a, is due to the intersection of two adjacent rays in a meridional cross section. The full focal curve is a circle around the axis in a plane perpendicular to the axis. The phase shift due to these focal lines of a ray Φ_{Fa} is the same as for a circular cylinder and given by Eq. (7.14). For a spherical particle, the point where a ray interacts the axis is a focal line, noted as set b, because corresponding rays in other meridional sections have the same point of intersection. The full focal line is the full axis, both before and beyond the sphere. The phase due to these focal lines are

$$\Phi_{Fb} = \frac{\pi}{2}\left[-2k_p + \frac{1}{2}(1-q_p)\right], \tag{7.20}$$

where k_p and q_p are determined from Eq. (7.10). The total phase shift due to the focal lines of the ray of order p is the summation of the Φ_{Fa} and Φ_{Fb}.

To determine the divergence factor of a sphere, we consider an incident beam of section dA_i illuminating an area $dA = a^2\cos\tau d\tau d\phi$ on the sphere. All the flux in the beam, after interaction with the particle, spreads into a solid angle $d\Omega$ which corresponds to a surface $dA_s = r^2 d\Omega = r^2\sin\theta d\theta d\phi$ in far distance r from the sphere. According to the balance of energy, the scattered intensity of order p is given by

$$I_p(\theta) = \frac{\varepsilon_{X,p}^2 I_0 a^2 \sin\tau\cos\tau d\tau d\phi}{r^2\sin\theta d\theta d\phi} = \frac{a^2}{r^2} I_0 \varepsilon_{X,p}^2 D, \tag{7.21}$$

where the divergence factor D is defined by

$$D = \frac{\sin\tau\cos\tau}{\sin\theta\,|d\theta/d\tau|}. \tag{7.22}$$

The derivative $d\theta/d\tau$ is given in Eq. (7.17). We find finally the divergence factor of order p in terms of incident and refraction angles as follows

$$D = \frac{\sin(2\theta_i)}{4\sin\theta\left(p\dfrac{\tan\theta_r}{\tan\theta_i} - 1\right)} = \frac{\sin(2\theta_i)}{4\sin\theta\left(p\dfrac{\cos\theta_i}{m\cos\theta_r} - 1\right)}. \tag{7.23}$$

In the special case of the external reflection (p = 0), the deviation angle $\theta = \pi - 2\theta_i$, the divergence factor is a constant equal to 1/4. The deviation angle of the refraction ray is $\theta = 2(\theta_r - \theta_i)$, the divergence factor for the refracted ray p = 1 is written as

$$D = \frac{\sin(2\theta_i)}{4\sin[2(\theta_r - \theta_r)]}\frac{m\cos\theta_r}{\cos\theta_i - m\cos\theta_r}. \tag{7.24}$$

These results will be applied in the next section to check the formulas of VCRM.

7.2.3. Comparison of Scattering Diagrams with Lorenz - Mie Theory

In this section we will present some scattering diagrams calculated by geometrical optics and compare them with the Lorenz - Mie theory to show its applicability.

The scattering diagrams of an infinite cylinder calculated by the geometrical optics described in the above section and by Lorenz - Mie theory for two different sizes are shown in Fig. 7.4. The incident wavelength is 0.6328 μm and the refractive index of the particle is 1.33. It is clear that when the size of the particle is much greater than the wavelength (a = 50 μm in Fig. 7.4(a)) the agreement between GO and the LMT is very satisfactory in almost all directions except in vicinity of rainbow angles. From Fig. 7.4(b) (a = 10 μm) we can see that the GO can predict correctly the scattering for particle of size about 10 times the wavelength.

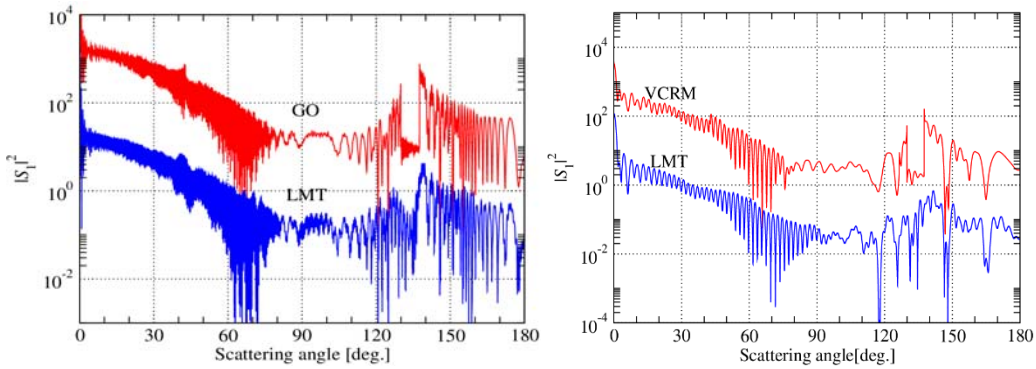

(a) a = 50 μm (b) a = 10 μm

Fig. 7.4. Comparison of the scattering diagrams computed by GO and LMT for an infinite circular cylinder of water (m = 1.33) of radius a illuminated by a plan wave of wavelength λ = 0.6328 μm. The results of LMT and GO are shifted by 10^{-2} and 10^2 respectively for clarity [13].

The geometrical optics can easily be extended to the scattering of shaped beam, called therefore Extended Geometrical Optics Approximation (EGOA) [7, 8]. When the divergence of the incident beam is small, we suppose that the rays in the particle propagate rectilinearly. In that case, we need only to take into account the local amplitude and phase of each ray at incident point. The incident angle is the angle between the normal of the particle surface and the normal of the incident wave front surface which is determined by the gradient of the phase function of the incident wave.

We compare in Fig. 7.5 the scattering diagrams calculated by EGOA and Generalized Lorenz - Mie theory (GLMT) for a spherical water droplet. The agreement is excellent in all directions and still better than the case of plane wave. This is because the waist radius of the incident beam is smaller than the radius of the particle and the intensity of the rays which contribute to scattering around the rainbow angles is much smaller than that on the axis.

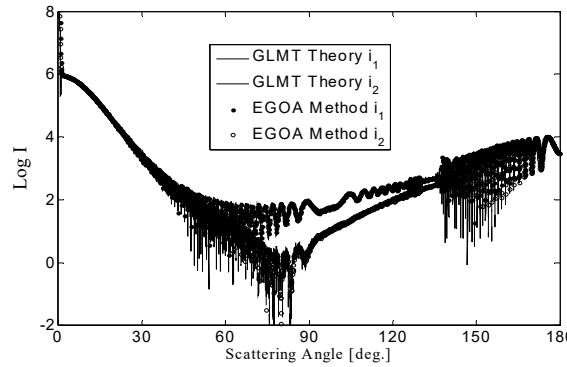

Fig. 7.5. Comparison of the scattering intensities calculated by GLMT and EGOA for a water droplet (m = 1.333) of radius a = 25 μm illuminated by a Gaussian beam of waist radius w_0 = 10 μm and wavelength λ = 0.6328 μm. The particle is located at the center of the beam.

7.3. Vectorial Complex Ray Model

We have seen in the previous section that, if the amplitude and the phase shifts of all the rays are correctly counted, the classical geometrical optics can predict the scattering of a wave by an infinite circular cylinder and a sphere with good precision when the particle size is large compared to the wavelength. This is based on the fact that the divergence factor and the phase shift due to the focal lines can be calculated analytically.

In the case where the particle has no such circular or spherical symmetry (referred in the following as non - spherical particle), the incident angle changes at each interaction of a ray with the particle surface. The divergence factor depends on the local curvature of the particle surface, the wave front curvature of the incident wave and the incident angle. No analytical expression of divergence factor is possible for arbitrarily shaped particle. We have shown also that these two properties cannot be achieved by pure numerical technique [14].

In principle, the phase shift due to focal lines is just a count of the passage of focal lines. Accordingly it is dependent on the convergence of the waves in and out of the particle. Therefore, to count correctly the variation of the amplitude of a ray and its phase shift due to the focal lines, we must be able to predict the curvature of the wave front of the wave that a ray represents.

In the Vectorial Complex Ray Model (VCRM) that will be presented in this section, the wave front curvature is considered as a new intrinsic property of a ray besides the four properties described in Section 7.2. Furthermore, in VCRM all properties of a ray: propagation direction, polarization, amplitude and phase will be described in vector, their components and complex numbers.

7.3.1. Snell Law and Fresnel Formulas in Vector Form

Knowing the fact that $k_\nu \sin\theta_\nu$ ($\nu = i,\ l$ or r represent respectively incident, reflected or refracted wave) is the tangent component of the wave vector $\boldsymbol{k}_\nu$ in the tangent plane to the diopter and $k_r = mk_i$, the Snell laws of reflection and refraction (7.1) and (7.2) can be written simply as

$$k_{i\tau} = k_{l\tau} = k_{r\tau}, \tag{7.25}$$

where the index τ stands for the tangent component. The normal components of the reflected and refracted waves are respectively $k_{ln} = -k_{in}$ and $k_{rn} = \sqrt{k_r^2 - k_{i\tau}^2}$.

Similarly, since $k_\nu \cos\theta_\nu$ is the component of the wave vector in the normal direction of the diopter surface, the Fresnel formulas (7.3)-(7.6) can therefore be written as function of the normal components of wave vectors

$$r_\perp = \frac{k_{in} - k_{rn}}{k_{in} + k_{rn}}, \tag{7.26}$$

$$t_\perp = \frac{2k_{in}}{k_{in} + k_{rn}}, \tag{7.27}$$

$$r_\parallel = \frac{m^2 k_{in} - k_{rn}}{m^2 k_{in} + k_{rn}}, \tag{7.28}$$

$$t_\parallel = \frac{2mk_{in}}{m^2 k_{in} + k_{rn}}. \tag{7.29}$$

When the total reflection occurs, the tangent component of the incident wave vector is greater than the wave number of the refracted wave $k_\tau > k_r$. The normal component of the refracted wave becomes a pure imaginary number if the two media are both transparent. By taking into account the time convention, it can be written as $k_{rn} = -i\sqrt{k_{i\tau}^2 - k_r^2}$. The

Fresnel coefficients become complex. Therefore, the phase shifts due to the reflection and refraction vary, in general, as function of the incident angle and must be counted correctly in the phase calculation of the rays.

It is worth to note that though Eqs. (7.25)-(7.29) are equivalent to Eqs. (7.1)-(7.6) they are much more convenient to the numerical calculation, especially for the scattering of 3D irregular particles since only four basic operations are necessary.

7.3.2. Wave Front Equation

When a wave arrives on a curved surface, the reflected wave and the refracted wave will be converged or diverged according to the curvature of the surface, i.e. the wave front curvature will change and the amplitude of the emergent wave in far field will be more or less important. To describe this property, we introduce the wave front curvature as a new property of a ray. By matching the phase between the incident wave and the reflected or refracted wave, we can establish the wave front equation. The derivation of this equation is tedious and will be omitted here. We will focus our attention to its physical interpretation and applications.

Consider an arbitrary wave whose wave front curvature at the incident point is described by the curvature matrix Q in the base ($\boldsymbol{t}_1$, $\boldsymbol{t}_2$) (Fig. 7.6)[1]. The curvature of the dioptric surface is given by the curvature matrix C in its base ($\boldsymbol{s}_1$, $\boldsymbol{s}_2$). The curvature matrix of the wave after refraction or reflection Q' is given by the wave front equation [9]

$$\left(\boldsymbol{k}_r - \boldsymbol{k}\right)\cdot \boldsymbol{n}C = k_r \Theta'^T Q' \Theta' - k_i \Theta^T Q \Theta \,, \tag{7.30}$$

where the letters with prime represent the quantities after refraction or reflection, the superscript T the transpose of the matrix, Θ the projection matrix between the unitary vectors of the coordinates systems on the planes tangent to the wave front ($\boldsymbol{t}_1$, $\boldsymbol{t}_2$) and the dioptric surface ($\boldsymbol{s}_1$, $\boldsymbol{s}_2$)

$$\Theta = \begin{pmatrix} \boldsymbol{t}_1 \cdot \boldsymbol{s}_1 & \boldsymbol{t}_1 \cdot \boldsymbol{s}_2 \\ \boldsymbol{t}_2 \cdot \boldsymbol{s}_1 & \boldsymbol{t}_2 \cdot \boldsymbol{s}_2 \end{pmatrix}. \tag{7.31}$$

In the case of the plane wave scattering by an ellipsoid or when the axis of an axis - symmetric beam passes by the symmetric axis of the ellipsoid, the rays in the plane defined

---

[1] When ($\boldsymbol{t}_1$, $\boldsymbol{t}_2$) are the principal directions of the wave front, the matrix Q is diagonal and may be written as $Q = \begin{pmatrix} 1/R_1 & 0 \\ 0 & 1/R_2 \end{pmatrix}$, where R_1 and R_2 are the principal curvature radii of the wave front. Similar notation is applied to the dioptric surface. For example, the cuvature matrix C of a sphere of radius a is $C = \begin{pmatrix} 1/a & 0 \\ 0 & 1/a \end{pmatrix}$, and that of a infinite cylinder is $C = \begin{pmatrix} 1/a & 0 \\ 0 & 0 \end{pmatrix}$.

by the beam axis and the ellipsoid axis remain always in this plane for any orders. This is a special case but very interesting because it simplifies considerably the problem. It permits a good understanding of the essential concepts of VCRM and reveals certain physical phenomena.

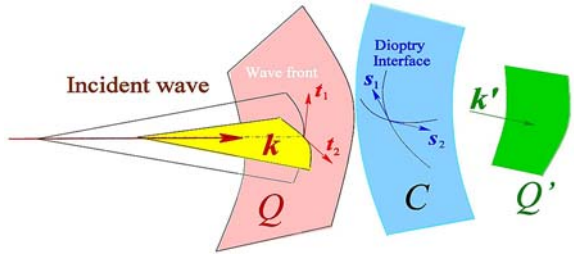

Fig. 7.6. Schema of the wave fronts and the dioptric surface.

Without loss of generality, we suppose that $\boldsymbol{s}_2$ and $\boldsymbol{t}_2$ are in the incident plane, that means $\boldsymbol{s}_1 \cdot \boldsymbol{t}_1 = 1$ and $\boldsymbol{s}_2 \cdot \boldsymbol{t}_2 = \cos\theta_i$. Similar relations can be found for the refracted wave. The wave front equation (7.30) is simplified to two scalar equations. The relation between the curvature radii in the plane perpendicular to the incident plane is given by [9, 10]:

$$\frac{k_r}{R_{r1}} = \frac{k_i}{R_{i1}} + \frac{k_{rn} - k_{in}}{\rho_1}, \tag{7.32}$$

and the relation of the curvature radii in the incident plane reads as:

$$\frac{k_{rn}^2}{k_r R_{r2}} = \frac{k_{in}^2}{R_{i2}} + \frac{k_{rn} - k_{in}}{\rho_2}, \tag{7.33}$$

where R stands for the curvature radius of the wave front and ρ that of the diopter. The index 1 and 2 indicate respectively the values in the plane perpendicular or parallel to the symmetric plane. It is important to note that the wave front curvature in the direction perpendicular to the scattering plane evolves also at each interaction with particle surface. This is different from the pure two dimension problem as an infinite cylinder of circular, elliptical or any other section shape.

7.3.3. Amplitude and Phase of a Ray

The amplitude of a ray may change during the propagation due to the convergence and divergence. In the case of light scattering of a plane wave by an infinite circular cylinder or by a sphere, the divergence factor has been introduced to describe the variation of the intensity (or amplitude) of the ray. A phase shift of focal line has also been calculated according to the suggestion of van de Hulst [1]. In the aforementioned cases, both the divergence factor and the total phase shift due to the focal lines are given in analytical

expressions. In the framework of VCRM for non spherical particle, these two properties are to be evaluated step by step according to the wave front curvature.

7.3.3.1. Amplitude

When a wave propagates from one point to another, its amplitude, therefore the intensity evolves according to the divergence of the wave and the distance between the two points. The relation of the intensities between points A and B along a ray can be deduced from the energy balance as shown in Fig. 7.7.

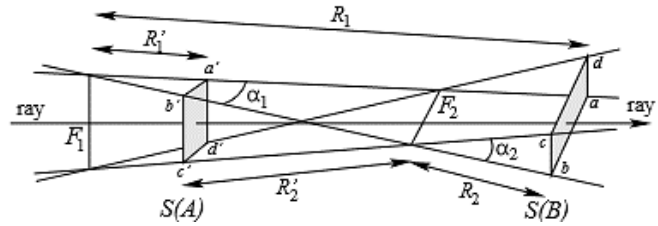

Fig. 7.7. Variation of pencil cross section and phase shift due to focal line.

The two focal lines are F_1 and F_2. We note the two principal radii of the curvature at A by $R_1^{'}$ and $R_2^{'}$, and those at B are R_1 and R_2, then the surface $a'b'c'd'$ at A is $S(A) = R_1^{'}\alpha_1 R_2^{'}\alpha_2$ and the surface $abcd$ at B is $S(B) = R_1\alpha_1 R_2\alpha_2$. The convergent or divergent characteristic of the wave can be noted by the sign of the curvature radii. In this chapter we adopt the convention that the curvature is positive if the focal line is after the considered point. Therefore, $R_2^{'}$ in Fig. 7.7 is positive while $R_1^{'}$, R_1 and R_2 are all negative. The sign of the curvature radii permits to count the phase of focal line that will be discussed later. For what concerns the intensity, only their absolute values matter. According to the conversation of energy, the energy flux passing through the surface $S(A)$ is equal to that through the surface $S(B)$, i.e. $I(A)[R_1^{'}\alpha_1 R_2^{'}\alpha_2] = I(B)[R_1\alpha_1 R_2\alpha_2]$. We deduce therefore

$$I(B) = I(A)\left|\frac{R_1^{'}R_2^{'}}{R_1 R_2}\right|. \tag{7.34}$$

In the light scattering by a particle, the intensity of the reflected wave at the first reflection is the product of the intensity of the incident wave on the particle surface I_0 and the intensity reflection ratio $\left|r_{X,0}\right|^2$. If we note the two radii of the reflected wave front by R_{11}^e and R_{21}^e, the scattered intensity at distance r is then

$$I(r) = I_0\left|r_{X,0}\right|^2\left|\frac{R_{11}^e R_{21}^e}{(r-R_{11}^e)(r-R_{21}^e)}\right|, \tag{7.35}$$

since the curvature radii of the reflected wave at distance r are $(r - R_{11}^e)$ and $(r - R_{21}^e)$.

Similarly, the intensity of the scattered light of order $p = 1$ is

$$I(r) = I_0 \left| t_{X,0} t_{X,1} \right|^2 \left| \frac{R_{11}^{'} R_{21}^{'}}{R_{11} R_{21}} \cdot \frac{R_{12}^e R_{22}^e}{(r - R_{12}^e)(r - R_{22}^e)} \right| \tag{7.36}$$

where the factors $t_{X,0}$ and $t_{X,1}$ are respectively the Fresnel transmission coefficient for $p = 0$ and 1. The term $\frac{R_{11}^{'} R_{21}^{'}}{R_{11} R_{21}}$ is the ratio of the intensities at two successive points.

In general, if we note the two curvature radii of the incident wave front at j^{th} interaction point by R_{1j} and R_{2j} ($j = 1, 2, \ldots, q$), those of the reflected or refracted wave by $R_{1j}^{'}$ and $R_{2j}^{'}$, and the two curvature radii of the emergent wave by R_{1j}^e and R_{2j}^e, then the intensity of the emergent ray after q interactions with the diopter is given by

$$I(r) = I_0 \left| \varepsilon_{X,p} \right|^2 D', \tag{7.37}$$

where $p = q - 1$ and the divergence factor D is defined by

$$D' = \left| \frac{R_{11}^{'} R_{21}^{'}}{R_{12} R_{22}} \cdot \frac{R_{12}^{'} R_{22}^{'}}{R_{13} R_{23}} \cdots \frac{R_{1q}^e R_{2q}^e}{(r - R_{1q}^e)(r - R_{2q}^e)} \right|. \tag{7.38}$$

The factor $\varepsilon_{X,p}$ is due to the reflection and refraction and given by

$$\varepsilon_{X,p} = \begin{cases} r_{X,0} & p = 0 \\ t_{X,0} t_{X,p} \prod_{i=1}^{p-1} r_{X,i} & p \geq 1 \end{cases}. \tag{7.39}$$

It is worth to note that $r_{X,0}$ is the Fresnel reflection coefficient on the surface outside of the particle while $r_{X,i}$ with $i \geq 1$ is the coefficient of the internal reflection. In the special case of light scattering of plane wave by an infinite circular cylinder or a spherical particle, the reflection coefficient is constant for all orders of rays. Eq. (7.39) is therefore reduced to Eq. (7.11).

The definition of the divergence factor (7.38) includes directly the size of the particle and is consistent to the divergence factor of the infinite circular cylinder and the sphere defined in Section 7.2. It includes already the prefactor a/r for the circular cylinder (see Eq. (7.18)) and a^2/r^2 for the sphere (see Eq. (7.23)). The detailed derivation of the divergence factor

of classical geometrical optics for the scattering of an infinite circular cylinder and a sphere from Eq. (7.38) will be given in the next subsection.

It is worth to point out that in light scattering theories, we talk often about the scattering diagram described by a function $F(\theta,\phi)$, such that (see Section 2.1 in [1])

$$I(\theta,\phi) = I_0 \frac{F(\theta,\phi)}{k^2 r^2}, \tag{7.40}$$

which is independent of *r* in far filed. In Lorenz - Mie theory for sphere, $F(\theta,\phi)$ is equal to $\left|S_1(\theta,\phi)\right|^2$ for perpendicular polarization and $\left|S_2(\theta,\phi)\right|^2$ for parallel polarization.

In VCRM, if we are interested only the scattering in far field, the term $(r - R_{1q}^e)(r - R_{2q}^e)$ is eliminated in the same way. The amplitude of scattered wave of order *p* is then calculated by

$$A_p = A_0 k \left|\varepsilon_{X,p}\right| \sqrt{D''}\,. \tag{7.41}$$

Where the new divergence factor is defined by

$$D'' = \left| \frac{R_{11}' R_{21}'}{R_{12} R_{22}} \cdot \frac{R_{12}' R_{22}'}{R_{13} R_{23}} \cdots R_{1q}^e R_{2q}^e \right|. \tag{7.42}$$

In the case of 2D, i.e. scattering by an infinite cylinder (circular, or elliptical or of any section shape), Eq. (7.41) is reduced to

$$A_p = A_0 \left|\varepsilon_{X,p}\right| \sqrt{\frac{\pi k}{2} \left| \frac{R_1'}{R_2} \cdot \frac{R_2'}{R_3} \cdots R_{1q}' \right|}, \tag{7.43}$$

since the convergence occurs only in one direction. The factor π/2 under the square root is necessary for the results to be consistent with LMT (see Eq. (8.40) in [15]).

7.3.3.2. Phase

The phase of rays plays a critical rule in counting the wave effect to predict the fine structure of the light scattering diagrams, such as the supernumerary bows, the fringes near the critical angle or the interference structure near different kinds of caustics. The phase of a ray in VCRM is counted in four parts:

The first is the phase due to optical path Φ_P which is computed directly according to the optical path, usually relative to a reference ray which arrives at the particle center in the same direction as the incident ray and goes out in the same direction as the emergent ray.

Let $\boldsymbol{r}_i$ and $\hat{\boldsymbol{k}}_i$ be respectively the position vector of i^{th} interaction point of the ray with particle surface and the normalized wave vector of the emergent ray from that point, the phase due to the optical path of a ray after q interactions with the particle is given by

$$\Phi_P = -k_0(\hat{\boldsymbol{k}}_0 \cdot \boldsymbol{r}_1 - \hat{\boldsymbol{k}}_q \cdot \boldsymbol{r}_q) - k_p \sum_{i=1}^{q-1} \hat{\boldsymbol{k}}_i \cdot (\boldsymbol{r}_{i+1} - \boldsymbol{r}_i), \tag{7.44}$$

where $\hat{\boldsymbol{k}}_0$ is the normalized wave vector of the incident ray. In the case of scattering of the plane wave by an infinite circular cylinder or a sphere, $\hat{\boldsymbol{k}}_0 \cdot \boldsymbol{r}_1 = -\hat{\boldsymbol{k}}_q \cdot \boldsymbol{r}_q = -a\cos\theta_i$. The equation (7.23) of the phase due to the optical path of geometrical optics is recovered.

The second concerns the phase due to the reflection Φ_R which is calculated directly according to the Fresnel coefficient as described in the previous section. If no total reflection occurs, only a constant phase π is added to the perpendicular component for any incident angle and to the parallel component if the incident angle is larger than the Brewster angle. When the total reflection occurs, the phase shifts depend on the incident angle and the phase shifts are to be calculated and added to both polarizations. This is responsible of the effects of the tunneling (Goos Hänchen's shift) [16].

As for the phase due to the focal line, it is easy to be calculated in VCRM, because we need only to count the number n_f of sign changes of the wave front curvature radii between successive interactions of ray with the particle surface. And the total phase shift is given by

$$\Phi_F = n_f \frac{\pi}{2}. \tag{7.45}$$

Finally, if the incident wave is a shaped beam, the phase of the incident wave Φ_i is also to be counted.

In conclusion, the total phase of a ray in VCRM is summation of four kinds of phase shifts:

$$\Phi = \Phi_P + \Phi_R + \Phi_F + \Phi_i. \tag{7.46}$$

The phase due to optical path is independent of polarization and divergence of the wave, while the computation of the phases of reflection and focal lines is delicate, especially for problems without symmetry (or simply called 3D scattering) since both depend on the polarization of the wave.

7.3.4. Simple Applications of the Wave Front Equation

We will apply the wave front equation obtained in the Section 7.3.2 in some special cases: first in the formation of image by a plane diopter and a spherical diopter, and then in the

determination of the divergence factor in the plane wave scattering by an infinite circular cylinder and a sphere. These examples show two aspects of applications of the wave front equation. They help also to understand different aspects of the equations.

7.3.4.1. Image Formation by a Plane Diopter

Consider a plane diopter which separates two media 1 and 2 of refractive indices equal respectively to m_1 and m_2 (Fig. 7.8). A point object A is in the medium 1 distant OA from the refraction point O. The curvature radius of the diopter being infinity, the distance of the image A' from the refraction point, according to Eq. (7.33), is given by

$$\frac{m_2 \cos^2 \theta_r}{\overline{OA}'} = \frac{m_1 \cos^2 \theta_i}{\overline{OA}} . \tag{7.47}$$

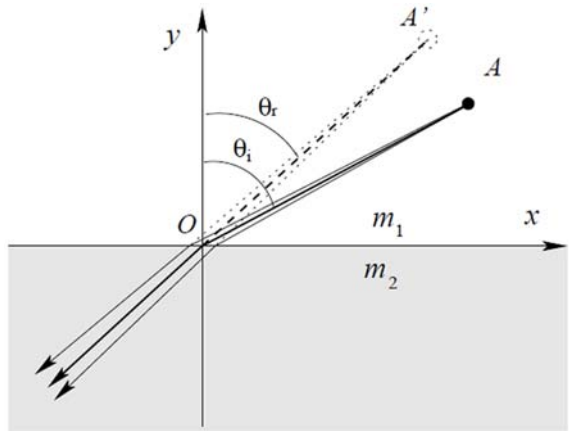

Fig. 7.8. Image formation by a plane diopter.

We note that $\overline{OA}$ and $\overline{OA}'$ have the same sign. This implies that the object and its image are in the same side of the diopter. Suppose that the coordinates of the object point A are (x, y). We can obtain the coordinates of the image point B according to Eq. (7.42)

$$x' = \frac{\cos^2 \theta_r}{\cos^2 \theta_i} x, \qquad y' = \frac{m_2 \cos^2 \theta_r}{m_1 \cos^2 \theta_i} y. \tag{7.48}$$

Therefore, both the lateral and longitudinal distances between the image and the object $x' - x$ and $y' - y$ depend on the incident angle θ_i. When the incident angle θ_i is small, the common conjugation relation of a plane diopter $\frac{m_1}{\overline{OA}} = \frac{m_2}{\overline{OA}'}$ is recovered. And only in this case the lateral shift $x' - x$ tends to 0, i.e. $x' \approx x$.

7.3.4.2. Image Formation by a Spherical Diopter

Consider a spherical diopter of radius a and center C separating two media of refractive indices m_1 and m_2 (Fig. 7.9). A point source A is placed on an axis passing by C.

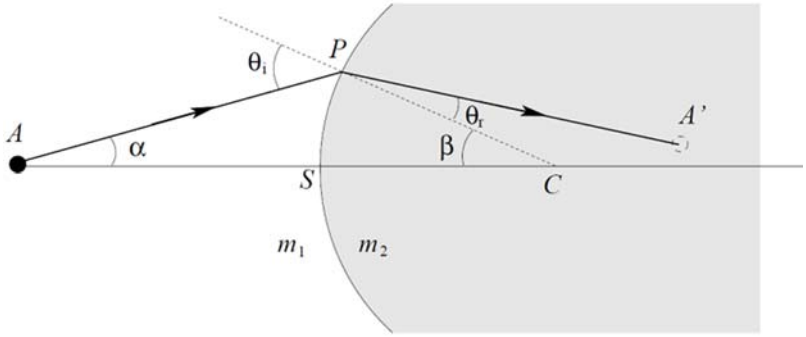

Fig. 7.9. Image formation by a spherical diopter.

In the paraxial case, i.e. for small θ_i, the commonly used conjugation relation

$$\frac{m_2}{\overline{SA'}} = \frac{m_{1i}}{\overline{SA}} + \frac{m_2 - m_1}{\overline{SO}}, \tag{7.49}$$

is found directly by either of Eq. (7.32) or Eq. (7.33). However, in general case, the two curvature radii of refracted wave are different. The image distance given by the wave front equation for the curvature radius in the incident plane (7.33) is

$$\frac{m_2 \cos^2 \theta_r}{\overline{PA_2'}} = \frac{m_1 \cos^2 \theta_i}{\overline{PA}} + \frac{m_2 \cos \theta_r - m_1 \cos \theta_i}{a}, \tag{7.50}$$

which indicates that the image is a focal line perpendicular to the incident plane at A_2'. Yet, the image distance given by the second wave front equation is

$$\frac{m_2}{\overline{PA_1'}} = \frac{m_1}{\overline{PA}} + \frac{m_2 \cos \theta_r - m_1 \cos \theta_i}{a}, \tag{7.51}$$

which means that the image is a focal line in the incident plane at A_1'. Consequently, the image formed by rays off - axis is deformed. This is the source of aberration. In fact, the wave front equation can be applied to any curved diopter, so it is a powerful tool to study the aberration of any curved surfaces. See Ref. [16] for detailed discussion on the aberration of imaging formation.

7.3.4.3. Divergence Factor of a Circular Cylinder

Consider an infinite circular cylinder of radius a illuminated perpendicularly by a plane wave. One of the principal directions of the surface of the cylinder is along the axis and the other is tangent to the surface and perpendicular the axis. The corresponding curvature radii are respectively ∞ and a. The two curvature radii of the plane wave are both infinite.

For the reflection, the normal component of the reflected wave vector is opposite to that of the incident wave $k_{rn} = -k_{in}$ or $\cos\theta_r = -\cos\theta_i$. From Eq. (7.33) it is ready to find the curvature radius in the incident plane of the reflected wave

$$R_{l1} = -\frac{a\cos\theta_i}{2}. \tag{7.52}$$

The negative sign signifies that the curvature center is on the other side of the emergent wave. The other curvature radius is ∞.

For the refraction, the curvature radius of the refracted wave in the incident plane R_{r1} is found directly from Eq. (7.33)

$$\frac{m\cos^2\theta_r}{R_{r1}} = \frac{m\cos\theta_r - m\cos\theta_i}{a}. \tag{7.53}$$

If the refractive index of the cylinder $m > 1$, the curvature radii are positive, i. e. the center of the refracted wave is in the same side of the cylinder axis. In the contrary, if $m < 1$ R_{r1} is negative, the wave center is in the opposite side of the cylinder axis.

From the curvature radii given above, we can deduce the divergence factor of a cylinder. For the reflection, the divergence factor is

$$D' = \frac{R_{r1}}{r - R_{i1}} = \frac{a}{r-a}\frac{\cos\theta_i}{2}, \tag{7.54}$$

and that of the refraction is

$$D' = \frac{R'_{r1}}{R_{i2}}\frac{R^e_{r2}}{r - R^e_{r2}} = \frac{a}{r-a}\frac{m\cos\theta_i\cos\theta_r}{2(\cos\theta_i - m\cos\theta_r)}. \tag{7.55}$$

Naturally, in the far field the divergence factors given by geometrical optics are recovered as it should be.

7.3.4.4. Divergence Factor of a Sphere

Similar to the infinite cylinder, we can also demonstrate that the divergence factor given by GO can be found as a special case in VCRM. For example, the two principal curvature radii of the reflected wave can be obtained by the wave front equations (7.32) and (7.33)

$$R_{10} = -\frac{a\cos\theta_i}{2}, \qquad R_{20} = -\frac{a}{2\cos\theta_i}. \tag{7.56}$$

The convergence factor for reflection is therefore $(r \to \infty)$ $D = \frac{1}{4}$.

We can also demonstrate that the divergence factor of a sphere given by GO for high order rays can be found from the formulism of VCRM. Though there is no difficulty in principle, the calculation is somewhat tedious and we will omit it here.

7.4. Applications of VCRM in Light Scattering

As a short review, we will give a very brief description of some remarkable results to show the power of VCRM. The detailed information may be found in the references therein.

7.4.1. Revisit of Airy Theory in Term of VCRM

We will apply VCRM to the scattering of a spherical particle. We are interested especially in the scattered intensity around the rainbow angles and compare the results of VCRM to the Airy theory since the latter is largely used in the particle granulometry.

We show first in Fig. 7.10 the scattering diagrams calculated with three different methods [17]. It is clear that the difference of the peak positions and the intensity maxima of supernumerary bows predicted by the Airy theory and the rigorous Debye theory [4] increases rapidly as function of the distance from the main peak of rainbow, especially for the second rainbow. Whereas the agreement between the results of VCRM and the Debye theory is very satisfactory except in the neighborhood of geometrical rainbow angle since the diffraction effect must be introduced in VCRM to remedy this flaw. The reason why the Airy theory differs from the rigorous theory is due to two approximations in that theory: 1). the cubic phase function is deduced from the relation of deviation angle in the vicinity of rainbow angle, but in the Airy integration, this variable is extended to infinity, and 2) the amplitude of the rays near the rainbow angle is assumed to be constant but this is certainly not true because the divergence factor tends to infinity at geometrical rainbow angle. In VCRM, the phase and the amplitude of each ray are calculated rigorously in the framework of ray model. The results are naturally better that that of Airy theory.

Furthermore, it worth to point out that in VCRM the same procedure can be applied directly to calculate the intensity of the supernumerary bows of a non - spherical particle. Examples will be given in the last section.

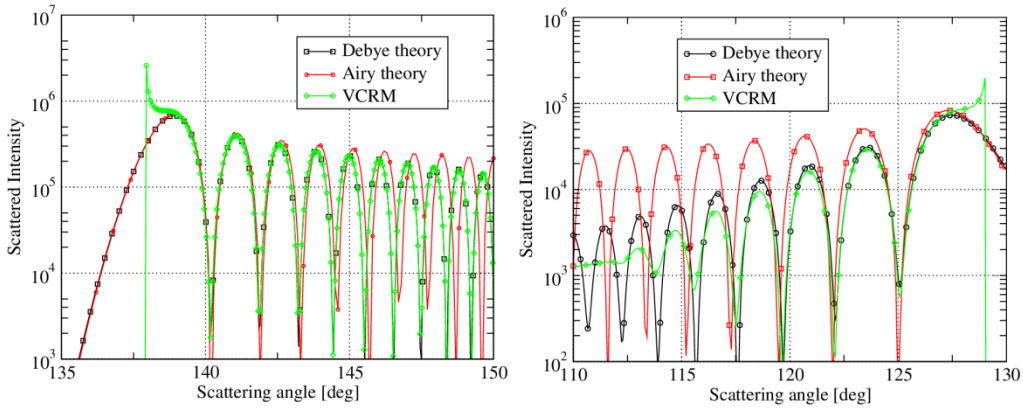

Fig. 7.10. Comparison of the scattered intensity calculated by Debye theory, Airy theory and VCRM for a spherical particle of water (m = 1.333) of radius a = 50 μm for the first order (left figure p = 2) and the second order (right figure p = 3) of rainbow.

7.4.2. Scattering by an Elliptical Cylinder

The scattering of a plane wave by an infinite elliptical cylinder at normal incidence is the simplest case of scattering by non - spherical particle since the convergence and divergence occur in one plane. Only one scalar wave front equation (7.33) is necessary. As an example, we show in Fig. 7.11 the scattering diagrams of an elliptical cylinder of semi - axis a = 50 μm along the incident direction and the other semi axis varies from 25 μm to 50 μm. The refractive index of the cylinder is 1.33 and the incident wavelength is λ = 0.6328 μm.

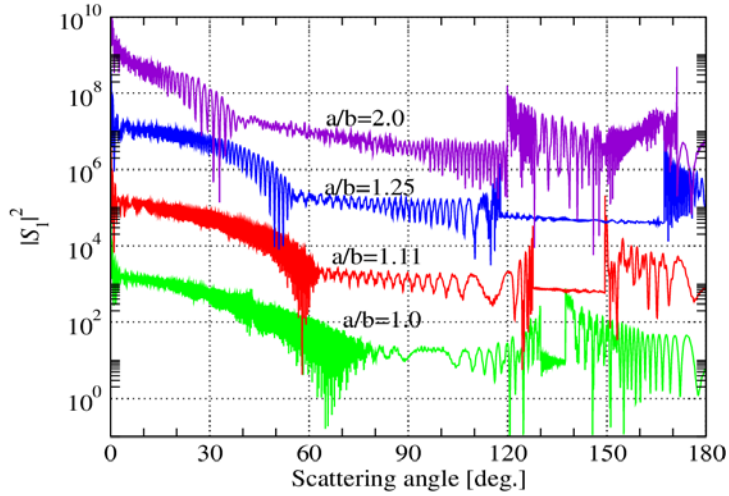

Fig. 7.11. Scattering diagrams of an elliptical cylinder illuminated by a plane wave for the different aspect ratios. The perpendicular polarization is chosen.

We find that when the aspect ratio a/b increases from 1 to 1.25, the first order rainbow goes to larger angle, the second order rainbow to the smaller angle and the Alexander region expands. When the aspect ratio is too big (a/b = 2.0 in the figure), the positions of the first rainbow (at 119.8°) and the second order rainbow (at 171.2°) are reversed.

VCRM is very easily to be extended to the scattering of a shaped beam. Fig. 7.12 shows the scattering diagrams of an elliptical cylinder at illuminated with a two dimensional Gaussian beam of different waist radius.

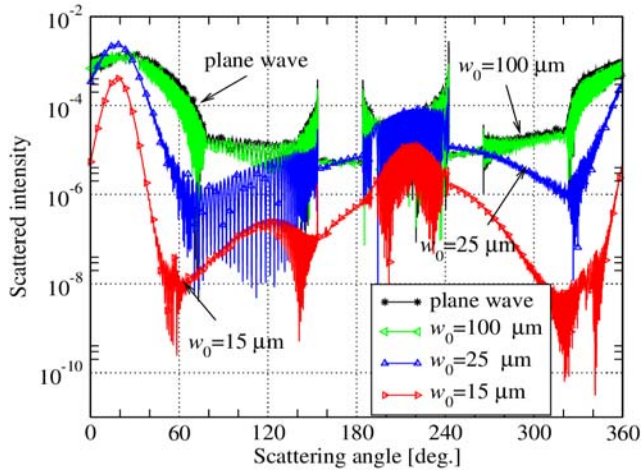

Fig. 7.12. Scattered diagrams of an elliptical cylinder of major radius a = 50 μm and minor radius b = 40 μm illuminated by plane wave and a two dimensional Gaussian beam of three different waist radius (w_0 = 100, 25, 15 μm). The incident beam is polarized along z direction and makes an angle θ_0 = 20◦ with x axis. The center of the beam is located on the axis of the cylinder [13].

The two semi - axes of the elliptical cylinder are respectively a = 50 μm and b = 40 μm and the incident wave is the plane wave or a two dimensional Gaussian beam of waist radius w_0 = 100 μm, 25 μm or 15 μm. The incident wave propagates in the direction x perpendicular to the axis of the cylinder z but makes an angle of 20° with the major axis of the elliptical section. We remark that the profile of the scattering diagrams are very different from those of the circular cylinder. The scattering diagrams are no longer symmetric, so they must be given in all directions (0 to 360°). The rainbow angles and the Alexander dark regions in the two sides of the scattering diagram (0◦ to 180◦ and 180◦ to 360◦) are not symmetric neither. When a cylinder is illuminated by a two dimensional Gaussian beam of waist radius relatively small, the incident beam intensity at the impact position for rainbow is weak. For example, in the case w_0 = 15 μm, the rainbow phenomena are not visible in two sides relative to the incident direction (20 to 200◦ and 200◦ to 20◦). If w_0 = 25 μm the rainbow is much visible in the side of scattering angle smaller than 200◦ than in the other side.

7.4.3. Scattering of the Plane Wave by an Ellipsoidal Particle

An ellipsoidal particle is a simple but very interesting model of non spherical particle [18, 19]. By changing the three semi - axes and incident angle we can investigate the influence of the curvature of the particle surface in different direction. To illustrate the essential characteristics of the scattering we will limit ourselves to the scattering of a plane wave in a symmetric plane of the particle.

All the calculations presented in this section have been done by the software VCRMEll2D which can be download from our website [20]. A FORTRAN version is also available by requiring the authors. The results of VCRM and these codes have been validated by comparison with a rigorous numerical method [21, 22].

7.4.4. Software VCRMEll2D

The software VCRMEll2D is composed of two modules, one for ray tracing and the other for the calculation of scattering diagram.

In the module of "`ray tracing`", apart from the properties of the particle, one can choose to illuminate whole or a portion of the particle with bundle of rays at a given angle. An example is shown in Fig. 7.13(a). This function permits to visualize the divergence and convergence of the wave in and out of the particle.

The module of "Scattering diagram" (Fig. 7.13(b)) permits to calculate the intensity of emergent rays for each order and the total scattering intensity. The diffraction in the forward direction can also be considered. Therefore, the interference is taken into account properly. The data of the scattering diagrams of each order and the total field are saved automatically in separated files. One can also choose to save all the properties of all the rays at each intersection point, including the coordinates of the point, the wave vectors, the Fresnel coefficients, the curvature radii of the diopter and the curvatures radii of the wave fronts of incident, reflected and refracted waves.

7.4.5. Hyperbolic Umbilic Foci of an Oblate Particle and Experimental Validation

The hyperbolic umbilic foci or the hyperbolic umbilic diffraction catastrophe of an oblate particle is a very interesting phenomenon in the light scattering and attracted attention of many researchers. It is, in fact, a deformation of rainbow in an oblate particle. Nye [23] and Marston et al [24] have given explanation to their formation of the skeleton in term of geometrical optics. Fig. 7.14 shows the photographs of rainbow region scattering patterns and the explanation of Marston. But the geometrical optics does not permit to predict the fine structure of the fringes in the scattering patterns.

To investigate these phenomena in the framework of VCRM and validate our model, an experiment has been realized [25, 26]. A droplet of Di - Ethyl - Hexyl - Sebacat (DEHS) is levated using acoustic pressure. The red curves in Fig. 7.15 show the measured scattering intensities around the first rainbow angles. The blue curves presents the

scattering diagrams calculated with VCRRMEll2D. It is clear that the VCRM predicts very well the fine structure in the rainbow region of an oblate.

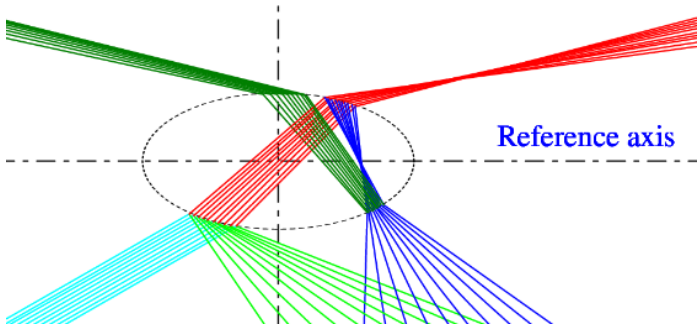

(a) Ray tracing in a spheroidal particle.

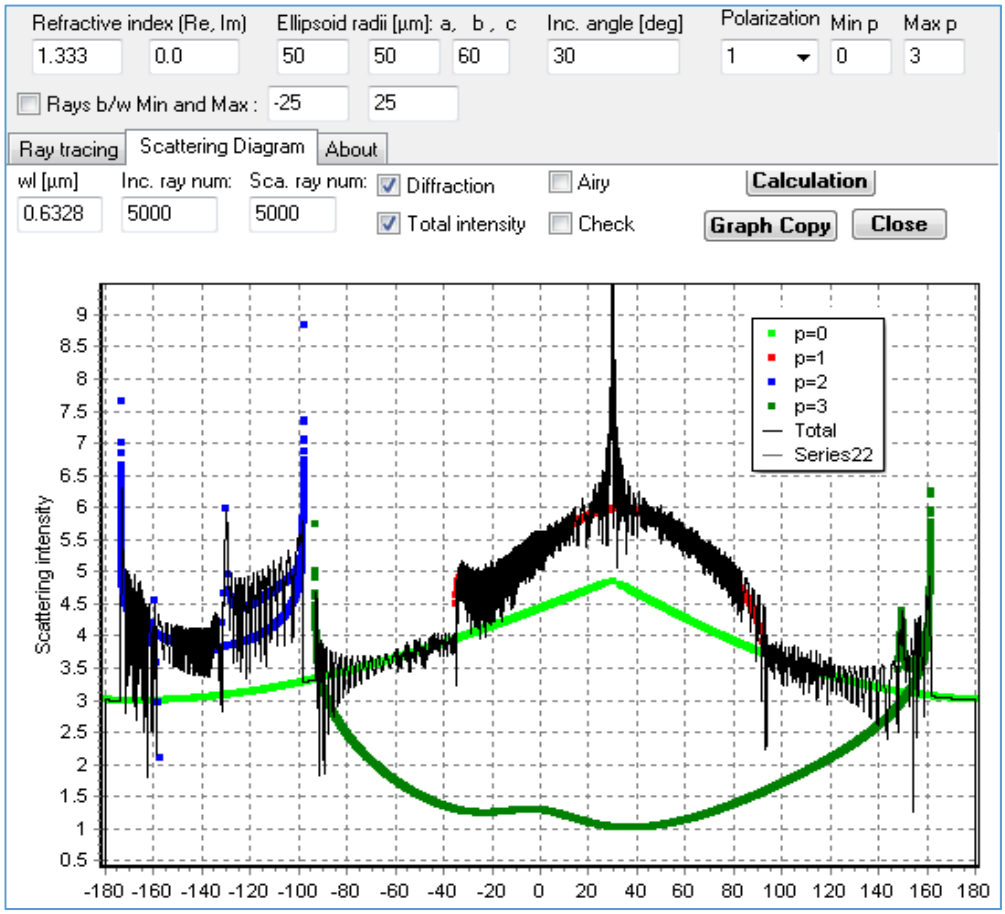

(b) Calculation of the intensity of each order and the total scattering diagram.

Fig. 7.13. Illustration of the software VCRMEll2D.

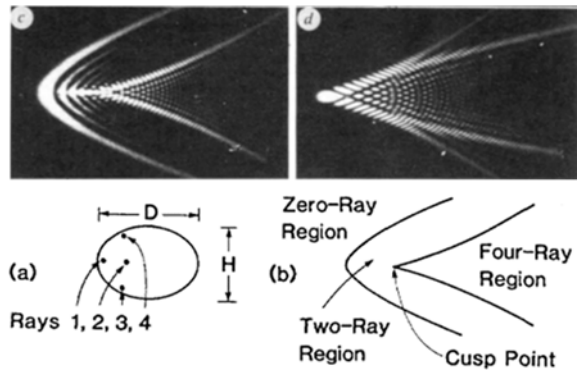

Fig. 7.14. Photographs of rainbow region scattering patterns (top) and explanation of Marston [24].

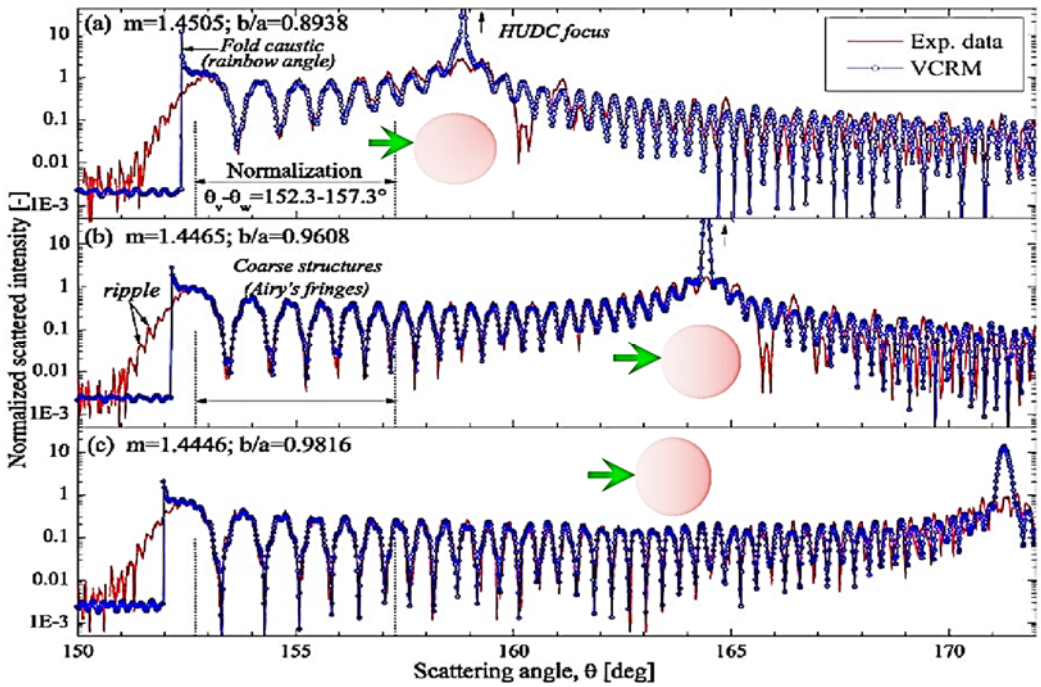

Fig. 7.15. Comparison of VCRM and experimental normalized equatorial scattering diagrams for the acoustically levated droplets of Di - Ethyl - Hexyl - Sebacat [25].

7.4.6. Dependence of Two Rainbow Intensity Ratio on the Aspect Ratio of a Prolate Particle

It is known that the intensity of the rainbow of a spherical particle decreases rapidly with the increasing of the order. The intensity of the second rainbow is about one magnitude weaker than the first rainbow. However, for a prolate particle, though the rainbow angles remain the same as a spherical particle of radius equal to the minor axis, the ratio between

the rainbow intensities of different orders varies as function of its aspect ratio. This is because the convergence of the wave in the direction along the major axis. As examples, we show in Fig. 7.16 the intensity diagram near the first and the second rainbows calculated by VCRMEll2D for a sphere and a prolate particle of two aspect ratios. The intensity ratio between the second rainbow and the first rainbow increases as function of the aspect ratio *c/a*. This property is very interesting to the characterization of non - spherical particle since it can be used to deduce the deformation of the particle [27].

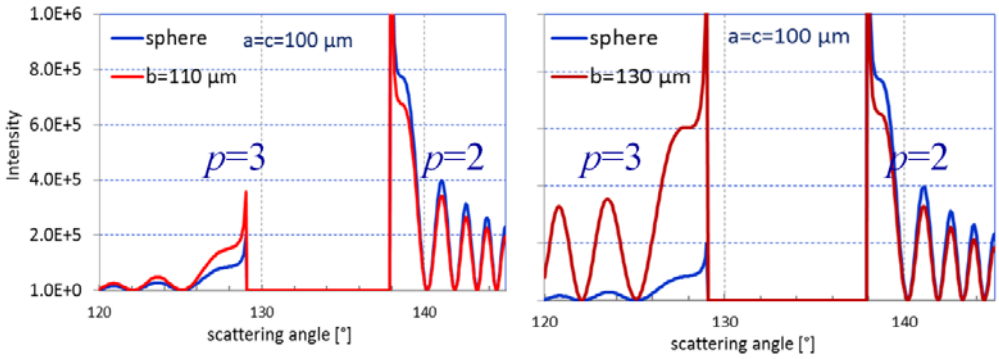

Fig. 7.16. Scattering intensities near the first and the second rainbows of a sphere and a prolate water droplet.

7.5. Conclusions

We have developed since a decade a novel model, called Vectorial Complex Ray Model (VCRM), to deal with the scattering of large non - spherical particle. The key originality of VCRM relies on the introduction of a new intrinsic property to describe the rays, i.e. the wave front curvature. This property, as well as four properties in the classical ray model (direction, amplitude, phase and polarization) evolves at each interaction of a ray with the particle surface and permits to evaluate precisely the amplitude and the phase of each ray so that to predict the scattering field with very good precision.

To ease the access of the new model, we begin with the simple cases of plane wave scattering by an infinite circular cylinder and a sphere. The essential concepts and the fundamental laws of VCRM are then presented along with simple applications to help the understanding.

Some remarkable results have been exampled to illustrate the power of VCRM. We have shown that VCRM predicts much better the positions and the amplitudes of supernumerary bows than the Airy theory of rainbow, which has been largely used in the measurement of refractive index and size of spherical particle. The infinite elliptical cylinder is the simplest non - spherical particle. We have illustrated that its scattering diagram are very sensible to the aspect ratio and the waist radius of the incident Gaussian beam.

Finally, the free software VCRMEll2D has been presented and applied to the scattering of a spheroidal particle. It is shown that VCRM predicts very well the fine structure in the rainbow (called also the hyperbolic umbilic diffraction catastrophe or hyperbolic umbilic foci) of an oblate particle. The intensity ratio between different rainbows is sensible to the aspect ratio of a prolate particle. VCRM can quantify this ratio and therefore be applied to the characterization of the deformation of droplets.

Acknowledgements

This work was funded by the French National Research Agency (ANR) under grants AMO - COPS (ANR - 13 - BS09 - 0008 - 01).

References

[1]. H. C. van de Hulst, Light Scattering by Small Particles, *Dover Publications*, 1957.
[2]. A. Macke, M. Mishchenko, K. Muinonen, B. Carlson, Scattering of light by large nonspherical particles: ray-tracing approximation versus T-matrix method, *Opt. Lett.,* Vol. 20, 1995, pp. 1934-1936.
[3]. M. I. Mishchenko, J. W. Hovenier, L. D. Travis, Light Scattering by Nonspherical Particles: Theory, Measurements and Applications, *Academic*, 2000.
[4]. E. Hovenac, J. Lock, Assessing the contributions of surface waves and complex rays to far - field Mie scattering by use of the Debye series, *J. Opt. Soc. Am. A*, Vol. 9, 1992, pp. 781-795.
[5]. P. Marston, Critical angle scattering by a bubble: physical - optics approximation and observations, *J. Opt. Soc. Am.*, Vol. 69, 1979, pp. 1205-1211.
[6]. P. Yang, K. Liou, Geometric-optics–integral-equation method for light scattering by nonspherical ice crystals, *Appl. Opt.*, Vol. 35, 1996, pp. 6568-6584.
[7]. F. Xu, K. Ren, X. Cai, Extension of geometrical-optics approximation to on-axis Gaussian beam scattering. I. By a spherical particle, *Appl. Opt.,* Vol. 45, 2006, pp. 4990-4999.
[8]. F. Xu, K. Ren, X. Cai, J. Shen, Extension of geometrical-optics approximation to on-axis Gaussian beam scattering. II. By a spheroidal particle with end - on incidence, *Appl. Opt*., Vol. 45, 2006, pp. 5000-5009.
[9]. K. F. Ren, F. Onofri, C. Rozé, T. Girasole, Vectorial complex ray model and application to two - dimensional scattering of plane wave by a spheroidal particle, *Opt. Lett.*, Vol. 36, Issue 3, 2011, pp. 370-372.
[10]. K. F. Ren, C. Rozé, T. Girasole, Scattering and transversal divergence of an ellipsoidal particle by using Vectorial Complex Ray Model, *J. Quant. Spectrosc. Radiat. Transfer*, Vol. 113, 2012, pp. 2419-2423.
[11]. A. Ungut, G. Grehan, G. Gouesbet, Comparisons between geometrical optics and Lorenz - Mie theory, *Appl. Opt.*, Vol. 20, 1981, pp. 2911-2918.
[12]. F. Xu, X. Cai, K. F. Ren, Geometrical - optics approximation of forward scattering by coated particles, *Appl. Opt.*, Vol. 43, Issue 9, 2004, pp. 1870-1879.
[13]. K. Jiang, Theoretical study of light scattering by an elliptical cylinder, PhD Thesis, *University of Rouen*, France, 24 June 2013.
[14]. Y. Yuan, Diffusion de la lumière par un objet irrégulier pour l'application à l'imagerie des sprays, PhD Thesis, *University of Rouen*, 29 March 2012.
[15]. C. F. Bohren, D. R. Huffman, Absorption and Scattering of Light by Small Particles, *J. Wiley and Sons*, New York, 1983.
[16]. M. Born, E. Wolf, Principles of Optics, 7th Ed., *Cambridge University Press*, 1999.

[17]. K. F. Ren, Airy theory revisited and caustics in vectorial complex ray model, in *Proceedings of the 7th World Congress on Particle Technology (WCPT'14),* Beijing, China, May 2014.
[18]. J. Lock, Ray scattering by an arbitrarily oriented spheroid. I. Diffraction and specular reflection, *Appl. Opt.*, Vol. 35, 1996, pp. 500-514.
[19]. J. Lock, Ray scattering by an arbitrarily oriented spheroid. II. Transmission and cross - polarization effects, *Appl. Opt.,* Vol. 35, 1996, pp. 515-531.
[20]. AMOCOPS, http://www.amocops.eu/
[21]. M. Yang, Y. Wu, X. Sheng, K. F. Ren, Comparison of scattering diagrams of large non - spherical particles calculated by VCRM and MLFMA, *J. Quant. Spectrosc. Radiat. Transfer*, Vol. 162, 2015, pp. 143-153.
[22]. M. Yang, Computation of light scattering, radiation force, torque and stress of large non - spherical particles with multilevel fast multipole algorithm and Vectorial Complex Ray Model, PhD Thesis, *University of Rouen*, 9 December 2014.
[23]. J. F. Nye, Rainbow scattering from spheroidal drops - an explanation of the hyperbolic umbilic foci, *Nature*, Vol. 312, Issue 5994, 1994, pp. 531-532.
[24]. P. L. Marston, E. H. Trinh, Hyperbolic umbilic diffraction catastrophe and rainbow scattering from spheroidal drops, *Nature*, Vol. 312, Issue 5994, 1984, pp. 529-531.
[25]. M. P. L. Sentis, F. R. A. Onofri, L. Méès, S. Radev, Scattering of light by large bubbles: coupling of geometrical and physical optics approximations, *J. Quant. Spect. Rad. Trans.*, Vol. 170, 2016, pp. 8-18.
[26]. K. F. Ren, F. R. A. Onofri, M. Yang, X. Sheng, The fine structure in the scattering diagrams of large ellipsoidal particle predicted by Vectorial Complex Ray Model, in *Proceedings of the 9th International Symposium on Measurement Techniques for Multiphase Flows (ISMTMF'15)*, Sapporo, Japan, Sept. 2015.
[27]. K. F. Ren, C. Roze, S. Idlahcen, Z. Ma, Observation of exotic scattering patterns of suspended droplets and their theoretical prediction by Vectorial Complex Ray Model, in *Proceedings of the 27th Annual Conference on Liquid Atomization and Spray Systems (ILASS-Europe'16)*, Brighton, United Kingdom, Sept. 2016.